Available online at www.sciencedirect.com
ScienceDirect
Journal of Sound and Vibration 323 (2009) 826–848
JOURNAL OF SOUND AND VIBRATION
www.elsevier.com/locate/jsvi

Evaluation of dynamic vehicle axle loads on bridges with different surface conditions

Lina Ding[a], Hong Hao[a], Xinqun Zhu[b,*]

[a]School of Civil and Resource Engineering, The University of Western Australia, Crawley, WA 6009, Australia
[b]School of Engineering, University of Western Sydney, Building XB, Kingswood Campus, Locked Bag 1797, Penrith South, DCNSW 1797, Australia

Received 15 October 2008; received in revised form 28 January 2009; accepted 29 January 2009
Handling Editor: L.G. Tham
Available online 17 March 2009

Abstract

Vehicles generate moving dynamic loads on bridges. In most studies and current practice, the actions of vehicles are modelled as moving static loads with a dynamic increase factor, which are obtained mainly from field measurements. In this study, an evolutionary spectral method is presented to evaluate the dynamic vehicle loads on bridges due to the passage of a vehicle along a rough bridge surface at a constant speed. The vehicle–bridge interaction problem is modelled in two parts: the deterministic moving dynamic force induced by the vehicle weight, and the random interaction force induced by the road pavement roughness. Each part is calculated separately using the Runge–Kutta method and the total moving dynamic load is obtained by adding the forces from these two parts. Two different types of vehicle models are used in the numerical analysis. The effects of the road surface roughness, bridge length, vehicle speed and axle space on the dynamic vehicle loads on bridges are studied. The results show that the road surface roughness has a significant influence on the dynamic vehicle–bridge interaction. The dynamic amplification factor (DAF) and dynamic load coefficient (DLC) depend on the road surface roughness condition.

1. Introduction

The bridges are dynamically loaded when vehicles travel on them. In practice, usually a moving static load is used to model the vehicle force on bridges. The static vehicle loads are, however, increased by a dynamic amplification factor (DAF) to account for the dynamic effects from the vehicle vibrations due to the interaction between the vehicle and bridge. Some codes define the DAF as a value between 0 and 0.4 for different vehicle type, such as the design code in Australia [5]. Other codes define it as a function of bridge span length, such as the AASHTO code [1]. These approaches avoid dynamic response analysis of the vehicle vibrations when moving along the bridge, and allow for a straightforward estimation of the vehicle loads in the bridge design. However, in reality the dynamic load due to the interaction between the vehicle and bridge is a complex problem and affected by many factors such as vehicle speed, road surface roughness, and dynamic

*Corresponding author. Tel.: +61 02 47360826; fax: +61 02 47360833.
E-mail addresses: lina@civil.uwa.edu.au (L. Ding), hao@civil.uwa.edu.au (H. Hao), xinqun.zhu@uws.edu.au (X. Zhu).

0022-460X/$ - see front matter © 2009 Elsevier Ltd. All rights reserved.
doi:10.1016/j.jsv.2009.01.051

properties of both the vehicle and bridge. Defining a DAF value based only on the vehicle type or the bridge span length might not lead to a reliable prediction of the dynamic loads on the bridges. In fact values of the DAF obtained from different references are quite different as discussed by Pesterev et al. [23] and Ashebo et al. [3].

Since the available field test data is limited and the test is costly, numerous theoretical derivations and numerical simulations have been carried out to calculate the bridge responses to vehicle loads. For example, with the assumption that the mass of the vehicle is small as compared to the mass of the bridge so that the interaction effect between the vehicle and bridge is insignificant, some researchers modelled the vehicle load as a static force moving along the bridge at a constant speed [26,12,7,24]. Other researchers modelled the vehicle as a moving mass when the inertia force of the vehicle mass cannot be ignored [2,6]. To account for the dynamic effects of the vehicle vibration when travelling along the bridge, dynamic vehicle models with different number of degrees-of-freedom (DOF) have also been developed to analyse the interaction between the vehicle and bridge [27,14,18,19].

The vehicle dynamic response is induced when it travels along an uneven road surface. In most previous studies [27,14,18,19], the road surface roughness history was simulated by inverse Fourier transform of the roughness power spectral density (PSD) function. The dynamic behaviour of the vehicle–bridge interaction was calculated using deterministic approaches. The limitation of these approaches is that the simulated roughness profile is only one realization of the randomly varying road surface roughness, which is therefore not sufficient to describe the possible road surface roughness effect on vehicle–bridge interaction. In the study by Hwang and Nowak [17], Chatterjee et al. [8], and Au et al. [4], Monte Carlo simulation was used to generate a set of road surface profiles to consider the randomness of the road surface roughness. The simulation was also carried out by inverse Fourier transform of the roughness spectral density function, and the vehicle–bridge interaction was solved in the time domain. Hwang and Nowak [17] used 2-D truck models and a continuous Euler-Bernoulli beam model in their study, and also considered the uncertainties of the truck type, total weight, axle distances, and speed. Chatterjee et al. [8] studied the coupled vertical–torsional dynamic response of multi-span suspension bridges due to vehicular movement, and considered 2D and 3D vehicle models. In the study by Chan et al. [9,10] the shell with eccentric beam element was used to model the bridge, and a 3D vehicle model considering both pitching and twisting modes was used to simulate the moving vehicle. The results were validated with field test. Comprehensive parametric calculations were carried out. However, the vehicle–bridge interaction was also solved in the time domain with the road surface roughness profiles simulated by inverse Fourier transform of the roughness spectral density function.

The road surface roughness is essentially random in nature and is assumed to have properties of a stationary process. Therefore, the vehicle–bridge interaction is also random. A few models have been proposed for evaluating the dynamic force in random nature. Fryba [11] investigated the non-stationary random vibration of a beam subjected to a moving random force. The statistical characteristics of the first and second order moment of the deflection and bending moment of the beam were calculated by the correlation method. Zibdeh [28] investigated the random vibration of a simply supported elastic beam subjected to random forces moving with time-varying velocity. Li et al [20] developed an approach for analysing the evolutionary random response of a coupled vehicle–bridge system. The vehicle is taken as a 2-DOF mass–spring system and the bridge is taken as a simply supported uniform beam. Lin and Weng [21] presented a spectral approach to evaluate the dynamic vehicle load due to the passage of a vehicle moving at a constant speed along the bridge. A one-quarter vehicle model is used in the analysis. The effects of vehicle speed and pavement roughness on the variation of dynamic vehicle load were investigated.

In this study, an evolutionary spectral approach for evaluating the dynamic deformation of the bridge and vehicle axle loads due to the passage of a vehicle moving along a rough bridge surface is developed. The input force to the bridge is divided into a deterministic part from the gravity of the vehicle and a random part related to the pavement roughness of the bridge. The road surface roughness is simulated by the displacement PSD provided by ISO 8608 [16]. Each part is calculated separately using the Runge–Kutta method. Results from a 2-DOF vehicle model moving on a simply supported uniform beam with a smooth surface [13] are used to calibrate the algorithm. The random response calculated with this model illustrates the influence of the road surface roughness on vehicle bridge interaction analysis. Then a more realistic 4-DOF vehicle model is

employed to study the dynamic response of the system. The results from the two vehicle models are compared and the reliability of each model in simulating vehicle–bridge interaction is discussed. The DAF and DLC are calculated to estimate the magnitude of the dynamic displacement of the bridge and the dynamic axle force. The effects of the vehicle speed, road surface roughness, vehicle axle spacing and bridge fundamental frequency on vehicle–bridge interaction are studied.

2. Formulation of the vehicle and the bridge model

In this study, the response of the bridge and vehicle are described by two separate sets of equations, which are coupled by the interaction force at the location of their contact point. The equations are then combined to form a fully coupled system. The system varies with time due to the vehicle moving along the bridge and vibrating in the vertical direction. The system equations are solved step by step in the time domain.

2.1. Vehicle model

The equation of motion of the vehicle system with respect to the vertical DOF $\mathbf{Y} = [y_1 \ y_2 \ y_3 \ldots y_n]$ derived using Lagrange formulation can be expressed as follows:

$$\mathbf{M}_v\ddot{\mathbf{Y}} + \mathbf{C}_v\dot{\mathbf{Y}} + \mathbf{K}_v\mathbf{Y} = -\mathbf{F}_v^{\text{int}} \tag{1}$$

where $\mathbf{F}_v^{\text{int}}$ is the interaction force vector applied to the vehicle; $\mathbf{M}_v$, $\mathbf{C}_v$, $\mathbf{K}_v$ are the mass, damping and stiffness matrices of the vehicle, respectively. For the 4-DOF vehicle model shown in Fig. 1, the vertical displacement vector $\mathbf{Y}$ contains the DOF attached to the suspension $\mathbf{y}_\alpha$ and the rigid vehicle body $\mathbf{y}_\beta$. Correspondingly, Eq. (1) can be expressed as

$$\begin{bmatrix} \mathbf{M}_\alpha & \mathbf{0} \\ \mathbf{0} & \mathbf{M}_\beta \end{bmatrix} \begin{Bmatrix} \ddot{\mathbf{y}}_\alpha \\ \ddot{\mathbf{y}}_\beta \end{Bmatrix} + \begin{bmatrix} \mathbf{C}_s & -\mathbf{C}_s \\ -\mathbf{C}_s & \mathbf{C}_s \end{bmatrix} \begin{Bmatrix} \dot{\mathbf{y}}_\alpha \\ \dot{\mathbf{y}}_\beta \end{Bmatrix} + \begin{bmatrix} \mathbf{K}_s & -\mathbf{K}_s \\ -\mathbf{K}_s & \mathbf{K}_s \end{bmatrix} \begin{Bmatrix} \mathbf{y}_\alpha \\ \mathbf{y}_\beta \end{Bmatrix} = -\begin{Bmatrix} \mathbf{0} \\ \mathbf{p} \end{Bmatrix} \tag{2}$$

where

$$IIbf\, M_\alpha = \begin{bmatrix} m_v a_2^2 + \dfrac{I}{I} I_v S^2 & m_v a_1 a_2 - \dfrac{I_v}{S^2} \\ m_v a_1 a_2 - \dfrac{I_v}{S^2} & m_v a_1^2 + \dfrac{I_v}{S^2} \end{bmatrix}; \quad \mathbf{M}_\beta = \begin{bmatrix} m_1 & 0 \\ 0 & m_2 \end{bmatrix}$$

$$\mathbf{C}_s = \begin{bmatrix} c_{s1} & 0 \\ 0 & c_{s2} \end{bmatrix}; \quad \mathbf{K}_s = \begin{bmatrix} k_{s1} & 0 \\ 0 & k_{s2} \end{bmatrix}; \quad \mathbf{p} = \begin{bmatrix} p_1(t) & p_2(t) \end{bmatrix}^{\mathrm{T}}$$

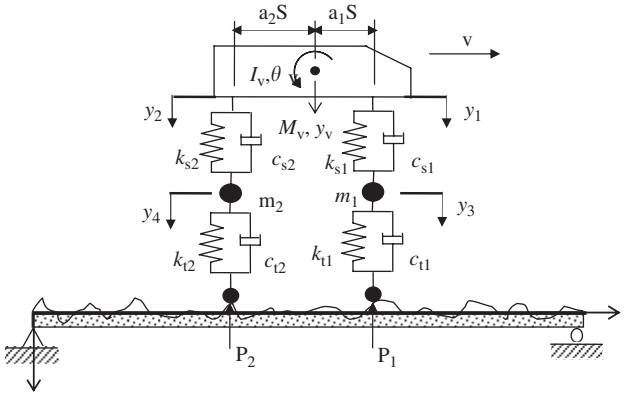

Fig. 1. Model of a coupled vehicle–bridge system.

in which m_v is the mass of the vehicle body; I_v is the moment of inertia of the vehicle body; S is the axle spacing; m_1 and m_2 are the masses of the two tyres; a_1 and a_2 are the position parameters; k_{s1} and k_{s2} are the stiffness of the suspension system; c_{s1} and c_{s2} are the damping of the suspension system; $p_1(t)$ and $p_2(t)$ are the interaction force between the vehicle and bridge. In this study, the simple vehicle model could be the interleaf spring system, but the effect of the interleaf friction is not considered.

2.2. Bridge model

The equations of motion for a bridge in the modal space can be expressed as

$$\ddot{\mathbf{q}} + \boldsymbol{\chi}\dot{\mathbf{q}} + \boldsymbol{\Omega}\mathbf{q} = M_n\boldsymbol{\Phi}^{\mathrm{T}}(\mathbf{f}_g + \mathbf{p}) \tag{3}$$

where

$$\mathbf{q} = [q_1(t)\ \ q_2(t)\ \ \ldots\ \ q_N(t)]^{\mathrm{T}};\quad \boldsymbol{\chi} = \mathrm{diag}\{2\xi_i\omega_i\};\quad \boldsymbol{\Omega} = \mathrm{diag}\{\omega_i^2\};\quad M_n = \frac{2}{m_b L}$$

$$\boldsymbol{\Phi} = \begin{bmatrix} \phi_1(\hat{x}_1(t)) & \phi_2(\hat{x}_1(t)) & \cdots & \phi_N(\hat{x}_1(t)) \\ \phi_1(\hat{x}_2(t)) & \phi_2(\hat{x}_2(t)) & \cdots & \phi_N(\hat{x}_2(t)) \end{bmatrix}^{\mathrm{T}};\quad \mathbf{f}_g = [(m_v a_2 + m_1)g\ \ (m_v a_1 + m_2)g]^{\mathrm{T}}$$

and where m_b is the mass per unit bridge length; L is the bridge length; $q_i(t)$ is the ith modal coordinate of the bridge; N is the number of the modes; ξ_i is the ith modal damping; ω_i is the undamped circular frequency; $\phi_i(\hat{x}_j(t))$ is the ith mode shape at $\hat{x}_j(t)$, the contact points between the wheels and bridge.

2.3. Vehicle–bridge interaction force

The interaction forces between the vehicle and the bridge are given by

$$p_1(t) = k_{t1}(y_3 - z_1) + c_{t1}(\dot{y}_3 - \dot{z}_1) \tag{4a}$$

$$p_2(t) = k_{t2}(y_4 - z_2) + c_{t2}(\dot{y}_4 - \dot{z}_2) \tag{4b}$$

where

$$z_l = w(\hat{x}_l(t), t) + r(\hat{x}_l(t)) \quad (l = 1, 2) \tag{5}$$

in which z_l is the vertical displacement of the wheel; $w(\hat{x}_l(t), t)$ and $r(\hat{x}_l(t))$ are the displacement and the road surface roughness of the bridge at the interaction point. Correspondingly, the derivative of z_1 and z_2 with respect to time is

$$\dot{z}_l = \dot{w}(\hat{x}_l(t), t) + w'(\hat{x}_l(t), t)\dot{\hat{x}}_l(t) + r'(\hat{x}_l(t))\dot{\hat{x}}_l(t) \tag{6}$$

where

$$w(\hat{x}_l(t), t) = \sum_{i=1}^{N} \phi_i(\hat{x}_l(t))q_i(t);\quad \dot{w}(\hat{x}_l(t), t) = \sum_{i=1}^{N} \phi_i(\hat{x}_l(t))\dot{q}_i(t)$$

$$w'(\hat{x}_l(t), t) = \sum_{i=1}^{N} \frac{\partial \phi_i(x)}{\partial x} q_i(t)\bigg|_{x=\hat{x}_l(t)};\quad \dot{\hat{x}}_l(t) = \frac{d\hat{x}_l(t)}{dt} \quad (l = 1, 2)$$

Substituting the above equations into Eqs. (4) and (5) results in

$$\mathbf{p} = \mathbf{K}_t\mathbf{y}_\beta + \mathbf{C}_t\dot{\mathbf{y}}_\beta - \mathbf{K}_t\mathbf{z} - \mathbf{C}_t\dot{\mathbf{z}} \tag{7}$$

$$\mathbf{z} = \boldsymbol{\Phi}\mathbf{q} + \mathbf{r} \tag{8}$$

with

$$\mathbf{C}_t = \begin{bmatrix} c_{t1} & 0 \\ 0 & c_{t2} \end{bmatrix}; \quad \mathbf{K}_t = \begin{bmatrix} k_{t1} & 0 \\ 0 & k_{t2} \end{bmatrix}; \quad \mathbf{z} = [z_1 \ \ z_2]^{\mathrm{T}}; \quad \mathbf{r} = \begin{Bmatrix} r(\hat{x}_1(t)) \\ r(\hat{x}_2(t)) \end{Bmatrix}$$

where k_{t1} and k_{t2} are stiffness of the tyres; c_{t1} and c_{t2} are damping of the tyres. Noting that for the vehicle travelling with a constant speed v, $\dot{\mathbf{\Phi}} = v\mathbf{\Phi}'$, and substituting Eq. (8) into Eq. (7) yields

$$\mathbf{p} = \mathbf{K}_t\mathbf{y}_\beta + \mathbf{C}_t\dot{\mathbf{y}}_\beta - (\mathbf{K}_t\mathbf{\Phi} + v\mathbf{C}_t\mathbf{\Phi}')\mathbf{q} - \mathbf{C}_t\mathbf{\Phi}\dot{\mathbf{q}} - \mathbf{K}_t\mathbf{r} - v\mathbf{C}_t\mathbf{r}' \tag{9}$$

2.4. Road surface roughness

In this study, the unevenness of the pavement is described by a roughness PSD as shown in Fig. 2, which is given by [16]

$$S_d(\Omega) = S_d(\Omega_0) \cdot (\Omega/\Omega_0)^{-\alpha} \tag{10}$$

where Ω is the spatial frequency in rad/m; Ω_0 is the reference angular spatial frequency equal to 1 (rad/m); and α is the parameter of the spectral shape taken as 2; $S_d(\Omega_0)$ is the roughness coefficient in m^2/rad/m. The road surface condition is classified into eight classes according to $S_d(\Omega_0)$. The Classes A to D describe the paved roadway condition and Classes E to H describe the unpaved roadway. Similar to the ISO classification for the normal road conditions, Honda et al. [15] tested 56 bridges and classified the bridge surface condition as very good, good, average and poor corresponding to the ISO specification Class A to C. Most of the bridge surfaces are in good to average condition. Table 1 gives the bridge surface roughness coefficient used in this study.

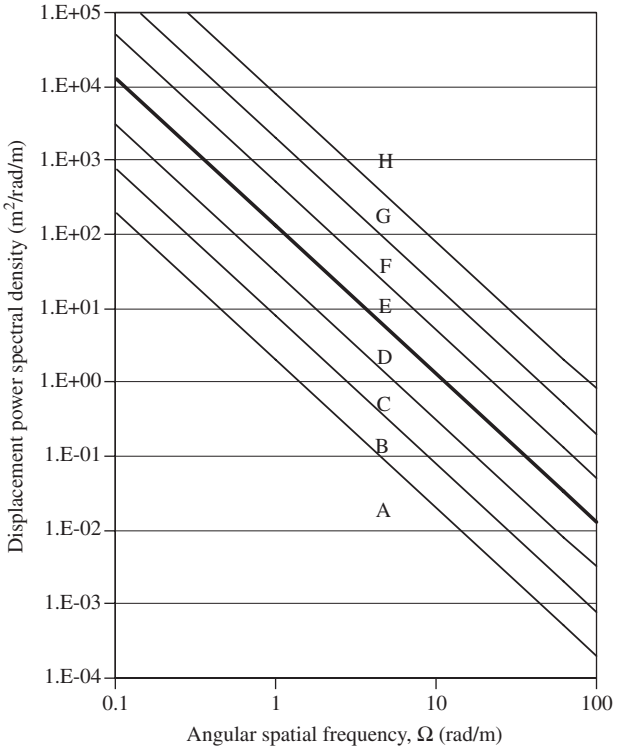

Fig. 2. Classification of the road.

Table 1
Road classification.

Road class	ISO (1995) [16] Honda et al. [15]	Very good	A Good	B Average	C Poor
$S_d(\Omega_0)$ (10^{-6} m^3/rad)	Lower limit	–	0.5	2	8
	Upper limit	0.5	2	8	32

3. Analysis of the dynamic interaction of the coupled vehicle–bridge system

3.1. Differential equations for the coupled vehicle–bridge system

With Eq. (9), Eqs. (2) and (3) can be combined together and written in a matrix form as follows:

$$\mathbf{M}\ddot{\mathbf{u}} + \mathbf{C}\dot{\mathbf{u}} + \mathbf{K}\mathbf{u} = \mathbf{f} \tag{11}$$

where

$$\mathbf{M} = \begin{bmatrix} \mathbf{I} & & \\ & \mathbf{M}_\alpha & \\ & & \mathbf{M}_\beta \end{bmatrix};$$

$$\mathbf{K} = \begin{bmatrix} \mathbf{\Omega} + M_n\mathbf{\Phi}^{\mathrm{T}}\mathbf{K}_t\mathbf{\Phi} + M_n v\mathbf{\Phi}^{\mathrm{T}}\mathbf{C}_t\mathbf{\Phi}' & \mathbf{0} & -M_n\mathbf{\Phi}^{\mathrm{T}}\mathbf{K}_t \\ \mathbf{0} & \mathbf{K}_s & -\mathbf{K}_s \\ -\mathbf{K}_t\mathbf{\Phi} - v\mathbf{C}_t\mathbf{\Phi}' & -\mathbf{K}_s & \mathbf{K}_s + \mathbf{K}_t \end{bmatrix}$$

$$\mathbf{C} = \begin{bmatrix} \mathbf{\chi} + M_n\mathbf{\Phi}^{\mathrm{T}}\mathbf{C}_t\mathbf{\Phi} & \mathbf{0} & -M_n\mathbf{\Phi}^{\mathrm{T}}\mathbf{C}_t \\ \mathbf{0} & \mathbf{C}_s & -\mathbf{C}_s \\ -\mathbf{C}_t\mathbf{\Phi} & -\mathbf{C}_s & \mathbf{C}_s + \mathbf{C}_t \end{bmatrix}$$

$$\mathbf{f} = \begin{Bmatrix} M_n\mathbf{\Phi}^{\mathrm{T}} \\ \mathbf{0} \\ \mathbf{0} \end{Bmatrix}\mathbf{f}_g + \begin{Bmatrix} -M_n\mathbf{\Phi}^{\mathrm{T}} \\ \mathbf{0} \\ \mathbf{I} \end{Bmatrix}\mathbf{K}_t\mathbf{r} + v\begin{Bmatrix} -M_n\mathbf{\Phi}^{\mathrm{T}} \\ \mathbf{0} \\ \mathbf{I} \end{Bmatrix}\mathbf{C}_t\mathbf{r}'$$

$$\mathbf{u} = [q_1 \;\; q_2 \;\; \ldots q_N \;\; y_1 \;\; y_2 \;\; y_3 \;\; y_4]^{\mathrm{T}}$$

The excitation $\mathbf{f}$ includes two parts, a deterministic excitation $\mathbf{f}_d$ due to the moving vehicle weight and a random excitation $\mathbf{f}_r$ due to vehicle vibration caused by the road surface roughness. They are expressed as

$$\mathbf{f}_d = \begin{Bmatrix} M_n\mathbf{\Phi}^{\mathrm{T}} \\ \mathbf{0} \\ \mathbf{0} \end{Bmatrix}\mathbf{f}_g; \quad \mathbf{f}_r = \begin{Bmatrix} -M_n\mathbf{\Phi}^{\mathrm{T}} \\ \mathbf{0} \\ \mathbf{I} \end{Bmatrix}\mathbf{K}_t\mathbf{r} + v\begin{Bmatrix} -M_n\mathbf{\Phi}^{\mathrm{T}} \\ \mathbf{0} \\ \mathbf{I} \end{Bmatrix}\mathbf{C}_t\mathbf{r}' \tag{12}$$

By introducing the state vector $\mathbf{z} = [\mathbf{u}^{\mathrm{T}} \;\; \dot{\mathbf{u}}^{\mathrm{T}}]^{\mathrm{T}}$, Eq. (11) can be rewritten as

$$\dot{\mathbf{z}}(t) = \mathbf{A}(t)\mathbf{z}(t) + \mathbf{b}_d(t) + \mathbf{b}_r(t)$$

where

$$\mathbf{A}(t) = \begin{bmatrix} \mathbf{0} & \mathbf{I} \\ -\mathbf{M}^{-1}\mathbf{K} & -\mathbf{M}^{-1}\mathbf{C} \end{bmatrix}; \quad \mathbf{b}_d(t) = \mathbf{M}_r\mathbf{f}_d; \quad \mathbf{b}_r(t) = \mathbf{M}_r\mathbf{f}_r; \quad \mathbf{M}_r = \begin{bmatrix} \mathbf{0} \\ \mathbf{M}^{-1} \end{bmatrix}$$

Because the inputs $\mathbf{f}_d$ and $\mathbf{f}_r$ are independent of each other and the system is linear, the responses corresponding to these excitations can be calculated separately.

3.2. Analysis of the response of the deterministic component

Consider the deterministic excitation due to the vehicle weight and let $\mathbf{b}_r$ equal 0, the coupled system equations are

$$\dot{\mathbf{z}}_d(t) = \mathbf{A}(t)\mathbf{z}_d(t) + \mathbf{b}_d(t) \tag{13}$$

Eq. (13) is a first order linear ordinary differential equation. It can be easily solved by numerical integration. The Runge–Kutta method is used in this study.

3.3. Analysis of the responses of the random component

The response equation for the random force is

$$\dot{\mathbf{z}}_r(t) = \mathbf{A}(t)\mathbf{z}_r(t) + \mathbf{b}_r(t) \tag{14}$$

Considering the random component, the particular solution to Eq. (14) is expressed as

$$\mathbf{z}_r(t) = \int_0^t \mathbf{H}(t,\tau)\mathbf{b}_r(t)\,\mathrm{d}\tau \tag{15}$$

Hence, the covariance matrix of $\mathbf{z}_r(t)$ can be expressed as

$$E[\mathbf{z}_r(t)\mathbf{z}_r^{\mathrm{T}}(t)] = \int_0^t \int_0^t \mathbf{H}(t,\tau)E[\mathbf{b}_r(\tau)\mathbf{b}_r^{\mathrm{T}}(\xi)]\mathbf{H}^{\mathrm{T}}(t,\xi)\,\mathrm{d}\tau\,\mathrm{d}\xi \tag{16}$$

where the covariance matrix of random excitation is

$$\begin{aligned} E[\mathbf{b}_r(\tau)\mathbf{b}_r^{\mathrm{T}}(\xi)] = {} & \mathbf{S}_k(\tau)E[\mathbf{r}(\tau)\mathbf{r}^{\mathrm{T}}(\xi)]\mathbf{S}_k(\xi) + \mathbf{S}_k(\tau)E[\mathbf{r}(\tau)\mathbf{r}'^{\mathrm{T}}(\xi)]\mathbf{S}_c(\xi) \\ & + \mathbf{S}_c(\tau)E[\mathbf{r}'(\tau)\mathbf{r}^{\mathrm{T}}(\xi)]\mathbf{S}_k(\xi) + \mathbf{S}_c(\tau)E[\mathbf{r}'(\tau)\mathbf{r}'^{\mathrm{T}}(\xi)]\mathbf{S}_c(\xi) \end{aligned} \tag{17}$$

where

$$\mathbf{S}_k(t) = \mathbf{M}_r \begin{Bmatrix} -M_n\boldsymbol{\Phi}^{\mathrm{T}} \\ \mathbf{0} \\ \mathbf{I} \end{Bmatrix} \mathbf{K}_t \quad \text{and} \quad \mathbf{S}_c(t) = \mathbf{M}_r \begin{Bmatrix} -M_n\boldsymbol{\Phi}^{\mathrm{T}} \\ \mathbf{0} \\ \mathbf{I} \end{Bmatrix} \mathbf{C}_t$$

With the derivation presented in Appendix A, Eq. (17) can be written as

$$\begin{aligned} E[\mathbf{b}_r(\tau)\mathbf{b}_r^{\mathrm{T}}(\xi)] = {} & \int_{-\infty}^{+\infty} [\mathbf{S}_k(\tau)\mathbf{S}_k^{\mathrm{T}}(\xi) + \mathrm{i}v\Omega\mathbf{S}_k(\tau)\mathbf{S}_c(\xi) - \mathrm{i}v\Omega\mathbf{S}_c(\tau)\mathbf{S}_k(\xi) \\ & + v^2\Omega^2\mathbf{S}_c(\tau)\mathbf{S}_c(\xi)]S_d(\Omega)\,\exp[\mathrm{i}\Omega(\hat{x}_1(\xi) - \hat{x}_1(\tau))]\,d\Omega \end{aligned} \tag{18}$$

Substituting Eq. (18) into Eq. (16) and changing the order of integration, Eq. (16) can be rewritten as

$$\begin{aligned} E[\mathbf{z}_r(t)\mathbf{z}_r(t)^{\mathrm{T}}] = {} & \int_{-\infty}^{+\infty} S_d(\Omega)\mathbf{Q}_1(t,\Omega)\bar{\mathbf{Q}}_1^{\mathrm{T}}(t,\Omega)\,d\Omega + \mathrm{i}v\int_{-\infty}^{+\infty} \Omega S_d(\Omega)\mathbf{Q}_1(t,\Omega)\bar{\mathbf{Q}}_2^{\mathrm{T}}(t,\Omega)\,d\Omega \\ & - \mathrm{i}v\int_{-\infty}^{+\infty} \Omega S_d(\Omega)\mathbf{Q}_2(t,\Omega)\bar{\mathbf{Q}}_1^{\mathrm{T}}(t,\Omega)\,d\Omega + v^2\int_{-\infty}^{+\infty} \Omega^2 S_d(\Omega)\mathbf{Q}_2(t,\Omega)\bar{\mathbf{Q}}_2^{\mathrm{T}}(t,\Omega)\,d\Omega \end{aligned} \tag{19}$$

where

$$\mathbf{Q}_1(t,\Omega) = \int_0^t \mathbf{H}(t,\tau)\mathbf{S}_k(\tau)\mathrm{e}^{-\mathrm{i}\Omega\hat{x}_1(\tau)}\,d\tau$$

$$\bar{\mathbf{Q}}_1(t,\Omega)=\int_0^t \mathbf{H}(t,\tau)\mathbf{S}_k(\tau)\mathrm{e}^{\mathrm{i}\Omega\hat{x}_1(\tau)}\,d\tau$$

$$\mathbf{Q}_2(t,\Omega)=\int_0^t \mathbf{H}(t,\tau)\mathbf{S}_c(\tau)\mathrm{e}^{-\mathrm{i}\Omega\hat{x}_1(\tau)}\,d\tau$$

$$\bar{\mathbf{Q}}_2(t,\Omega)=\int_0^t \mathbf{H}(t,\tau)\mathbf{S}_c(\tau)\mathrm{e}^{\mathrm{i}\Omega\hat{x}_1(\tau)}\,d\tau$$

Comparing the expression of $\mathbf{Q}_1(t,\Omega)$ with Eq. (15), $\mathbf{Q}_1(t,\Omega)$ for each constant Ω can be obtained by the Runge–Kutta method. Then the covariance matrix of system response can be calculate with Eq. (19) by integration with respect to Ω.

Similarly, the covariance matrix of input and output is obtained as

$$\begin{aligned}E[\mathbf{z}_r(t)\mathbf{b}_r^{\mathrm{T}}(t)]=\int_{-\infty}^{+\infty} & S_d(\Omega)\mathrm{e}^{\mathrm{i}\Omega vt}(\mathbf{Q}_1(t,\Omega)\mathbf{S}_k^{\mathrm{T}}(t)+\mathrm{j}v\Omega\mathbf{Q}_1(t,\Omega)\mathbf{S}_c^{\mathrm{T}}(t)\\ &-\mathrm{j}v\Omega\mathbf{Q}_2(t,\Omega)\mathbf{S}_k^{\mathrm{T}}(t)+v^2\Omega^2\mathbf{Q}_2(t,\Omega)\mathbf{S}_c^{\mathrm{T}}(t))\,d\Omega\end{aligned} \tag{20}$$

The covariance matrix of $\dot{\mathbf{z}}_r(t)$ can be expressed as

$$\begin{aligned}E[\dot{\mathbf{z}}_r(t)\dot{\mathbf{z}}_r^{\mathrm{T}}(t)]=&\mathbf{A}(t)E[\mathbf{z}_r(t)\mathbf{z}_r^{\mathrm{T}}(t)]\mathbf{A}^{\mathrm{T}}(t)+\mathbf{A}(t)E[\mathbf{z}_r(t)\mathbf{b}_r^{\mathrm{T}}(t)]+E[\mathbf{b}_r(t)\mathbf{z}_r^{\mathrm{T}}(t)]\mathbf{A}^{\mathrm{T}}(t)\\ &+E[\mathbf{b}_r(t)\mathbf{b}_r^{\mathrm{T}}(t)]\end{aligned} \tag{21}$$

3.4. Dynamic interaction force

For the deterministic part, the dynamic axle forces can be calculated with the following equations:

$$p_1(t)=-A_1\ddot{y}_1-A_2\ddot{y}_2-m_1\ddot{y}_3-(M_v a_2+m_1)g \tag{22a}$$

$$p_2(t)=-A_2\ddot{y}_1-A_3\ddot{y}_2-m_2\ddot{y}_4-(M_v a_1+m_2)g \tag{22b}$$

where

$$A_1=\left(m_v a_2^2+\frac{I_v}{S^2}\right);\quad A_2=\left(m_v a_1 a_2-\frac{I_v}{S^2}\right);\quad A_3=\left(m_v a_1^2+\frac{I_v}{S^2}\right)$$

For the random part, the covariance of axle loads is related with the vehicle acceleration covariance with the following equations.

$$\begin{aligned}E[p_1^2(t)]=&A_1^2E[\ddot{y}_1^2(t)]+A_2^2E[\ddot{y}_2^2(t)]+m_1^2E[\ddot{y}_3^2(t)]+2A_1A_2E[\ddot{y}_1(t)\ddot{y}_2(t)]\\ &+2A_1m_1E[\ddot{y}_1(t)\ddot{y}_3(t)]+2A_2m_1E[\ddot{y}_2(t)\ddot{y}_3(t)]\end{aligned} \tag{23a}$$

$$\begin{aligned}E[p_2^2(t)]=&A_2^2E[\ddot{y}_1^2(t)]+A_3^2E[\ddot{y}_2^2(t)]+m_2^2E[\ddot{y}_4^2(t)]+2A_2A_3E[\ddot{y}_1(t)\ddot{y}_2(t)]\\ &+2A_2m_2E[\ddot{y}_1(t)\ddot{y}_4(t)]+2A_3m_2E[\ddot{y}_2(t)\ddot{y}_4(t)]\end{aligned} \tag{23b}$$

3.5. Procedure of implementation

The responses of the coupled vehicle–bridge system consist of two components, deterministic part from gravity of the vehicle and random part generated from vertical vibrations of the vehicle owing to the road surface roughness. These two parts are calculated separately. The detailed procedure of implementation is:

Step 1: Calculate the frequencies and mode shapes of the bridge.
Step 2: Determine the mass, stiffness and damping matrices of both the vehicle and bridge and construct the coefficient matrix A according to Eqs. (11) and (12).

Step 3: Calculate the deterministic part by:

(i) Eq. (13) with Runge–Kutta method to obtain the displacement and velocity of the system and then substitute the results of $\mathbf{z}_d(t)$ back into Eq. (13) for accelerations of the system; and

(ii) Eq. (22) for the dynamic interaction forces.

Step 4: Calculate the random responses:

(i) $\mathbf{Q}_1(t,\Omega)$, $\bar{\mathbf{Q}}_1(t,\Omega)$, $\mathbf{Q}_2(t,\Omega)$ and $\bar{\mathbf{Q}}_2(t,\Omega)$ at each Ω with Runge–Kutta method;

(ii) the covariance of $\mathbf{z}_r(t)$ by integration over the frequency interval [0.06 18] as shown in Eq. (19);

(iii) the covariance of $\mathbf{b}_r(t)$ and $\mathbf{b}_r(t)\,\mathbf{z}_r(t)$ by Eqs. (18) and (20); and

(iv) the covariance of axle forces by Eq. (23).

4. Numerical simulations

4.1. Example 1: quarter vehicle model

To verify the proposed method, a dynamic analysis is performed first for a vehicle–bridge system available in the literature [13] as shown in Fig. 3, which is a 1-axle 2-DOF vehicle model moving at a constant speed along a simply supported beam. The parameters of the vehicle and beam are given in Table 2.

4.1.1. Deterministic response of the vehicle–bridge system

The road surface roughness is not considered in the latter study. Therefore, for comparison purpose, in this calculation, the smooth road surface condition is assumed. In Fig. 4(a), the time history of the mid-span displacement of the bridge by the proposed algorithm is compared with that from Green and Cebon [13] when the vehicle speed is 25 m/s. It shows that the results agree very well and therefore the proposed method is reliable to analyse the dynamic response of the coupled vehicle–bridge system.

Fig. 4(a) also shows the time history of the normalized mid-span displacement of the bridge when the vehicle speed is 15 and 35 m/s, in which δ is the mid-span displacement of the bridge and δ_{st} is the maximum static

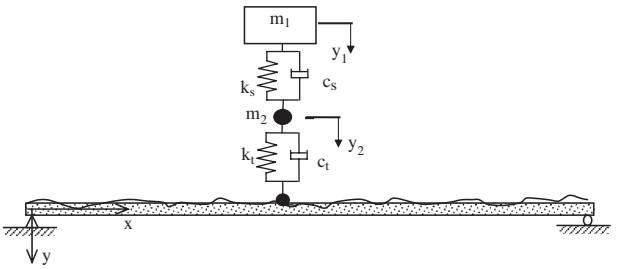

Fig. 3. A quarter car model moving on a simply supported bridge.

Table 2
Vehicle and bridge parameters.

Data of the bridge	Data of the 1-axle vehicle	Data of the 2-axle vehicle
$L = 40\,\text{m}$	$m_1 = 36\,000\,\text{kg}$	$m_v = 36\,000\,\text{kg}$
$m_b = 12\,000\,\text{kg/m}$	$m_2 = 4000\,\text{kg}$	$m_1 = m_2 = 2000\,\text{kg}$
$EI = 127\,500\,\text{MN m}^2$	$k_s = 1.8 \times 10^7\,\text{N/m}$	$I_v = 144 \times 10^3\,\text{kg m}^2$
	$k_t = 7.2 \times 10^7\,\text{N/m}$	$S = 2\,\text{m}$
	$c_s = 14.4 \times 10^4\,\text{N s/m}$	$a_1 = a_2 = 0.5$
	$c_t = 14.4 \times 10^4\,\text{N s/m}$	$k_{s1} = k_{s2} = 0.9 \times 10^7\,\text{N/m}$
		$k_{t1} = k_{t2} = 3.6 \times 10^7\,\text{N/m}$
		$c_{s1} = c_{s2} = 7.2 \times 10^4\,\text{N s/m}$
		$c_{t1} = c_{t2} = 7.2 \times 10^4\,\text{N s/m}$

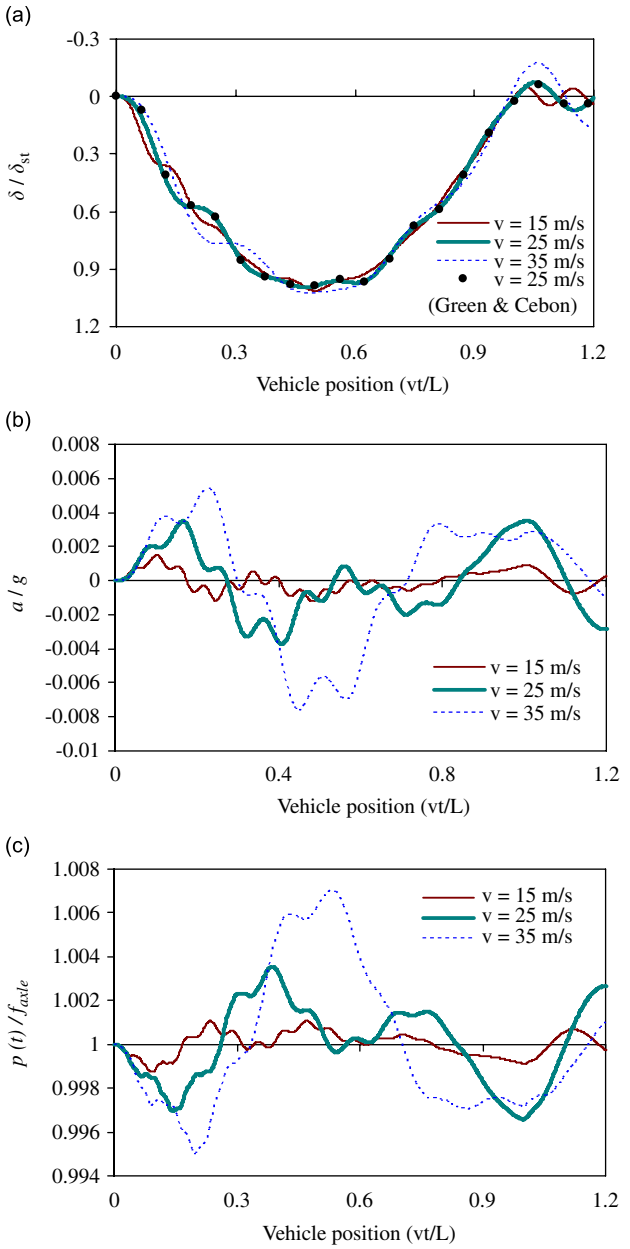

Fig. 4. Deterministic response of the vehicle–bridge system (quarter vehicle model): (a) displacement at the mid-span of the bridge; (b) vertical acceleration of vehicle body; and (c) vehicle axle forces.

displacement at the mid-span of the bridge under the same vehicle load. The static mid span displacement can be calculated from Eq. (24)

$$\delta_c = \frac{pb}{6EIL}\left[\frac{L}{b}\left(\frac{L}{2}-a\right)^3 - a^3 + (L^2-b^2)\frac{L}{2}\right] \quad a < \frac{L}{2} \tag{24a}$$

$$\delta_c = \frac{pb}{12EI}\left(\frac{3}{4}L^2 - b^2\right) \quad a \geqslant \frac{L}{2} \tag{24b}$$

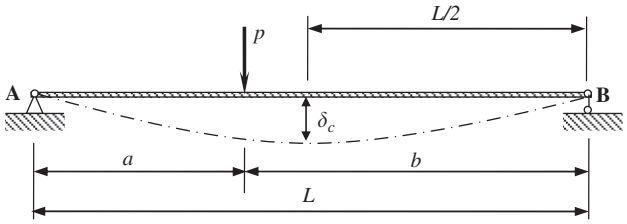

Fig. 5. Deformation of bridge under a concentrated load.

As shown in Fig. 5, p is the axle load; a and b are the distances from the loading point to the ends of the bridge. From Eq. (24), the maximum static displacement of the bridge occurs when b equals $L/2$, and is 4.14 mm for this case.

From Fig. 4(a), the time histories of the bridge displacement corresponding to different vehicle speeds are close to each other. The maximum displacements of the bridge are 1.01, 1.00 and 1.03 times δ_{st} for the three cases. The vehicle speed has no obvious effect on the bridge response for the smooth surface condition. Fig. 4(b) shows the vertical acceleration of the vehicle body when the vehicle is moving along the bridge. The maximum acceleration is 0.0015 g when the vehicle speed is 15 m/s, 0.0035 g when the speed is 25 m/s and 0.0053 g when the speed is 35 m/s. The results show that the acceleration of the vehicle body increases with the vehicle speed. The normalized time histories of axle loads are plotted in Fig. 4(c). In the figure, the interaction force oscillates around the static axle load f_{axle} or the vehicle weight. The peak–peak value of the oscillation increases with the vehicle speed. It should be noted that although the vehicle speed affects its vertical dynamic response, its effect is insignificant as compared to the static vehicle load or the weight of the vehicle on bridge responses. As shown in Fig. 4(b), the absolute maximum acceleration difference is only 0.014 g. This implies the total variation of the dynamic vehicle load is about 1.4 percent of its static load. Therefore, the displacement response shown in Fig. 4(a) is insensitive to the vehicle speed.

4.1.2. *Random response analysis of the vehicle–bridge system*

According to Honda et al. [15], the road roughness coefficient is taken as $2\times10^{-6}\,\mathrm{m^2/rad/m}$ for the upper limit of good road surface condition. Considering the random excitation due to the road surface roughness, the dynamic response of the vehicle–bridge system can be obtained by Eq. (14). The root-mean-square (RMS) response is used to describe the random response. The computation starts 40 m before the entrance of the bridge to obtain the stable vibration of vehicle. Using Eqs. (19) and (21), the RMS matrix of the response and the covariance matrix between the excitation and response can be obtained. To simplify the analysis, only the random response of the vehicle–bridge system due to the road surface roughness is studied in this section.

Fig. 6(a) shows the displacement at the mid span of the bridge when the vehicle is moving along the bridge at different speeds, namely 15, 25 and 35 m/s, respectively. The vertical axis is the normalized RMS value of the mid-span displacement of bridge. Fig. 6(b) shows the normalized RMS values of the vehicle body acceleration. Fig. 6(c) shows the normalized RMS value of the axle load, where f_{axle} is 392 kN. It is seen that the RMS values of all the response quantities in Fig. 6 increase with the vehicle speed. As shown in Fig. 6(a), the RMS value of the displacement at the mid-span of the bridge is $0.57\delta_{st}$ when the vehicle speed is 35 m/s, which is 1.5 times of the result when the speed is 15 m/s. This is because of the increase of the vertical acceleration response induced by the road surface roughness, which in turn results in a significant increase in the dynamic load. As shown in Fig. 6(b) and (c), the RMS values of the acceleration of the vehicle body increases from 0.18 to 0.28 g when the vehicle speed increases from 15 to 35 m/s, and the corresponding interaction force increases from 0.16 to 0.31 f_{axle}. These results show that the road surface roughness has a significant effect on the dynamic response of the vehicle–bridge system.

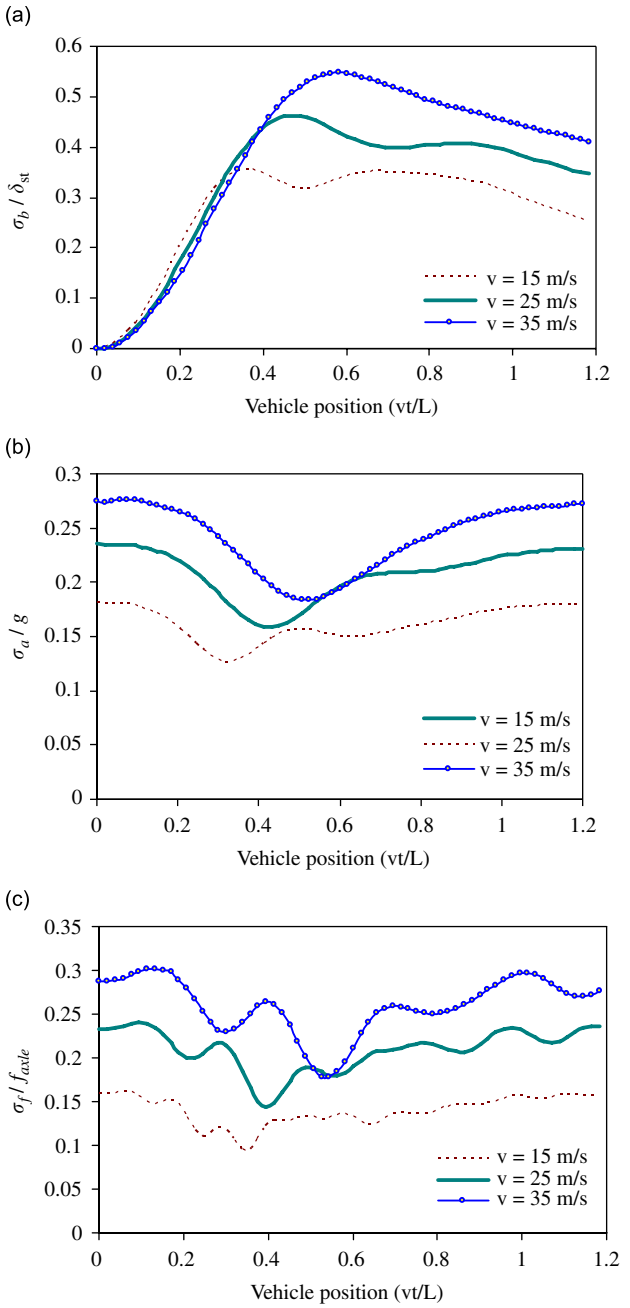

Fig. 6. RMS value of the dynamic response (quarter vehicle model): (a) the mid-span displacement of the bridge; (b) the vehicle body acceleration; and (c) the dynamic axle force.

4.2. Example 2: half vehicle model

In order to study the effect of the vehicle model on the numerical results, the vehicle in Example 1 is modelled as a 2-axle vehicle model with 4 DOF (as shown in Fig. 1). The parameters of the vehicle system are given in Table 2.

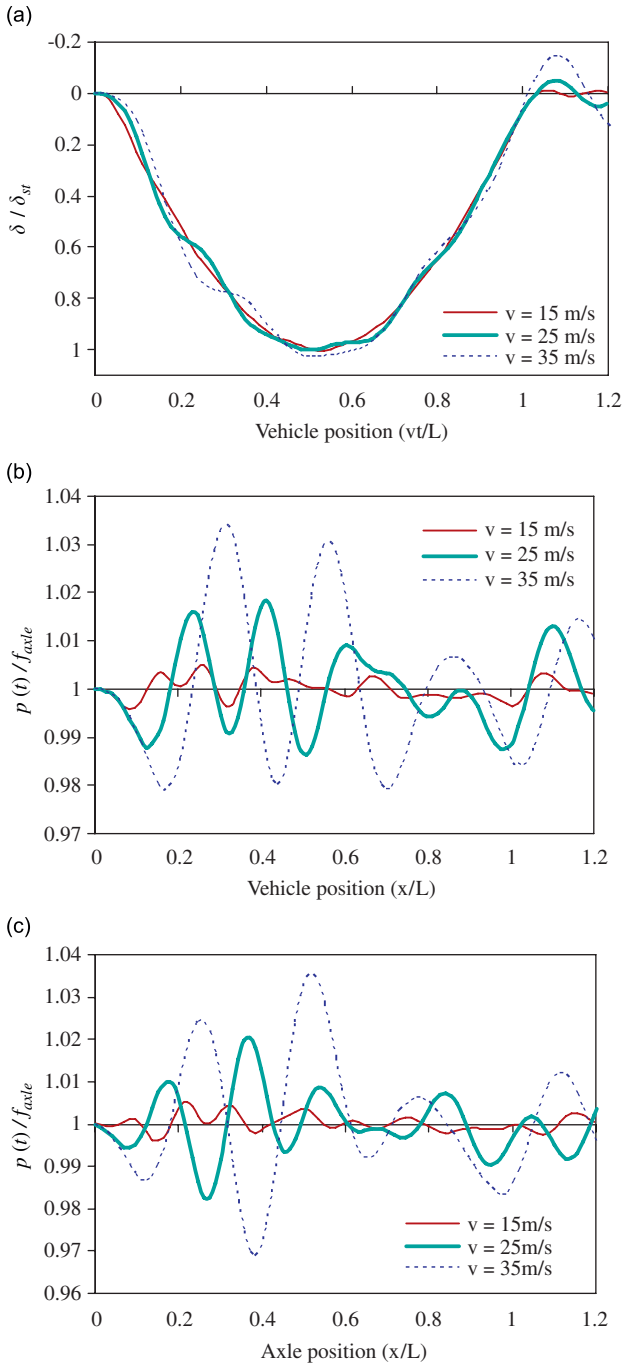

Fig. 7. Deterministic response of the vehicle–bridge system (half vehicle model): (a) displacement at the mid-span of the bridge; (b) front axle force; and (c) rear axle force.

4.2.1. Deterministic response of the vehicle–bridge system

Fig. 7(a) shows the displacement response at the mid-span of the bridge for different vehicle speeds, the corresponding front and rear axle loads are shown in Fig. 7(b) and (c). The vehicle position in Fig. 7(a) is described by the position of the front axle of the vehicle. The bridge surface is assumed to be smooth. δ_{st} for the half vehicle model is calculated with Eq. (24) by superposing the deflections from two concentrated loads.

The maximum static displacement usually occurs when the heavier axle is located at the mid-span of the bridge. In this example, both axles are assumed to carry the same weight, which induce a maximum bridge displacement of 4.10 mm. As shown again the normalized displacement time histories for different vehicle speeds are close to each other. The variance of the maximum displacements is less than 3 percent. In Fig. 7(b) and (c), the front and rear axle loads oscillate around the static axle load f_{axle}, which is 196 kN for both axles. The maximum axle load is 1.0.35 f_{axle} when the rear axle passes the 0.52 of the bridge length with a speed of 35 m/s. The dynamic effect causes the axle load to increase by 3.5 percent. These observations indicate again that the dynamic effect is insignificant when the bridge surface is smooth. Both vehicle models yield similar predictions when the road surface roughness is ignored.

4.2.2. *Random response analysis of the vehicle–bridge system*

The bridge road surface is assumed in good condition. The RMS values of bridge mid-span displacement and vehicle axle forces are plotted in Fig. 8. For comparison, the corresponding results of bridge displacement and vehicle axle load from the 2-DOF vehicle model are also shown in Fig. 8. It is seen that the effect of the road surface roughness on the bridge displacement and vehicle axle forces increase with vehicle speed for both vehicle model. Fig. 8(a) shows that the maximum dynamic RMS displacements of the bridge corresponding to the three vehicle speeds are $0.25\delta_{st}$, $0.33\delta_{st}$ and $0.39\delta_{st}$, respectively, for the 4-DOF vehicle model, indicating the maximum dynamic effect due to the road surface roughness results in 25, 33 and 39 percent increases in the bridge displacement for different speeds. Compared with the results from the 2-DOF vehicle model, which are $0.34\delta_{st}$, $0.47\delta_{st}$ and $0.57\delta_{st}$ for corresponding speeds, the normalized RMS displacement of the bridge decreases more than 35 percent.

In Fig. 8(b) and (c), the RMS dynamic axle loads for the front and rear axles are quite similar at each speed. The maximum normalized RMS dynamic axle loads acting on the bridge are 0.12, 0.16 and 0.19 when the vehicle speeds are 15, 25 and 35 m/s, respectively, which are more than 20 percent bigger than the corresponding axle forces from the 2-DOF model. The increment of axle forces and decrease of bridge displacements occur simultaneously, which can be explained with results in the frequency domain shown in Fig. 9.

As shown in Fig. 8(a), when the vehicle speed is 15 m/s, the maximum displacement of the bridge occurs when the vehicle locates at 0.36L for the 2-DOF vehicle model and 0.38L for the 4-DOF vehicle model. Fig. 9(a) shows the corresponding spectral density of the normalized maximum mid-span displacement of the bridge when the vehicle speed is 15 m/s. As shown there is only one peak value at 20 rad/s in displacement spectrum, occurring at the fundamental frequency of the bridge. Fig. 9(b) shows the spectral density of the normalized axle force. It is seen that spectral densities of the both vehicle models have peaks at 20 and 150 rad/s, which correspond to the vehicle bouncing mode and wheel hopping mode as shown in Fig. 10. In addition to these two peaks, there is another peak at 10 rad/s for the 4-DOF model which is the pitching mode of the vehicle. As shown the vehicle pitching mode at frequency 10 rad/s generates a larger axle force on the bridge, but the bridge response in this case is mainly induced by the axle force corresponding to the vehicle bouncing model at frequency 20 rad/s because of the resonance. Because of this, although the 4-DOF vehicle model gives a larger axle force than the 2-DOF vehicle model, larger bridge response is induced by the 2-DOF vehicle model.

The above observations indicate that the two vehicle models may give different numerical simulations of the vehicle–bridge interaction. Since the 2-axle 4-DOF vehicle model is more realistic, it is used in the subsequent analysis in this study.

5. Parametric study

The effect of the road surface roughness, vehicle speed, vehicle and bridge vibration frequencies and vehicle axle spacing on the vehicle–bridge interaction, and hence on the dynamic bridge responses are analysed in this section through two commonly used parameters in bridge design, i.e., the DAF and the dynamic load coefficient (DLC). The DLC is used to study the magnitude of the dynamic axle loads, which is defined as

$$\mathrm{DLC} = \frac{P_{\mathrm{dyn}}}{P_{\mathrm{st}}} \tag{25}$$

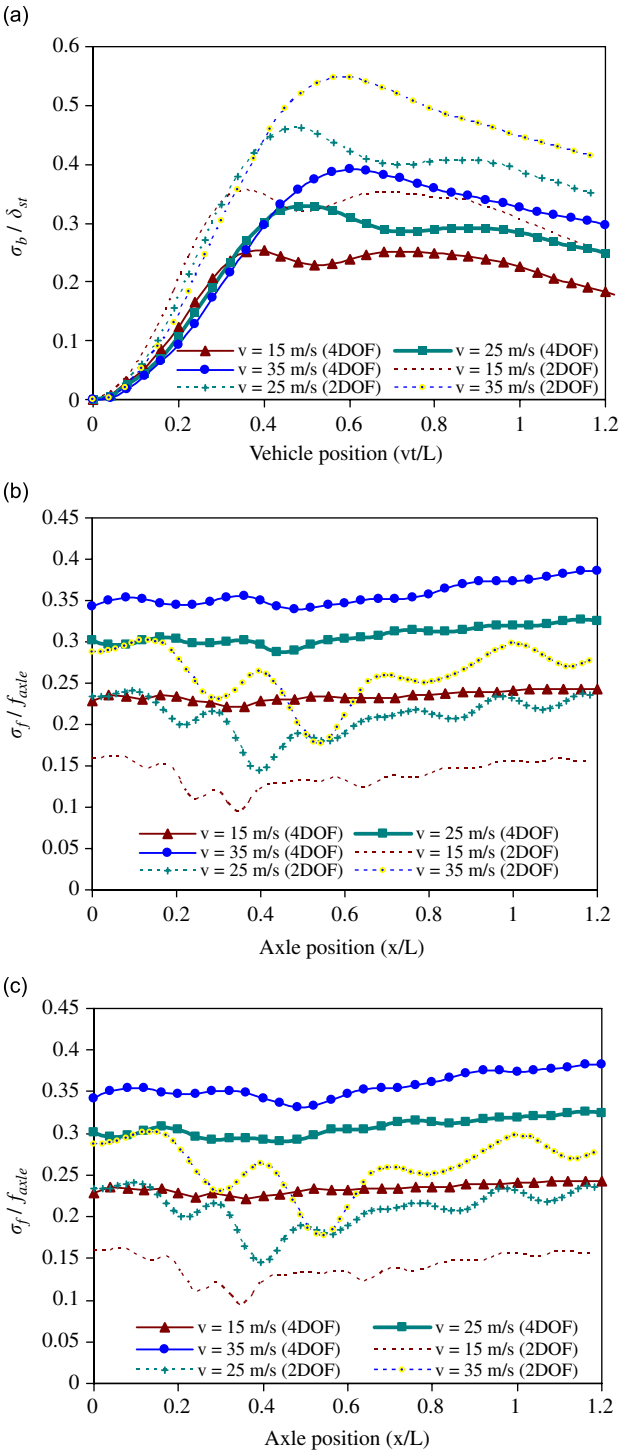

Fig. 8. RMS value of the dynamic response (half vehicle model): (a) RMS value of the mid-span displacement of the bridge; (b) RMS value of the dynamic axle force at front axle; and (c) RMS value of the dynamic axle force at rear axle.

P_{dyn} is the maximum value of the axle load, including the static axle load and the maximum RMS value of the dynamic axle load; P_{st} is the static axle load. The DAF is defined in terms of the dynamic response of the bridge, as the ratio of the maximum bridge deflection δ_{dyn} to the maximum static deflection δ_{st} under static

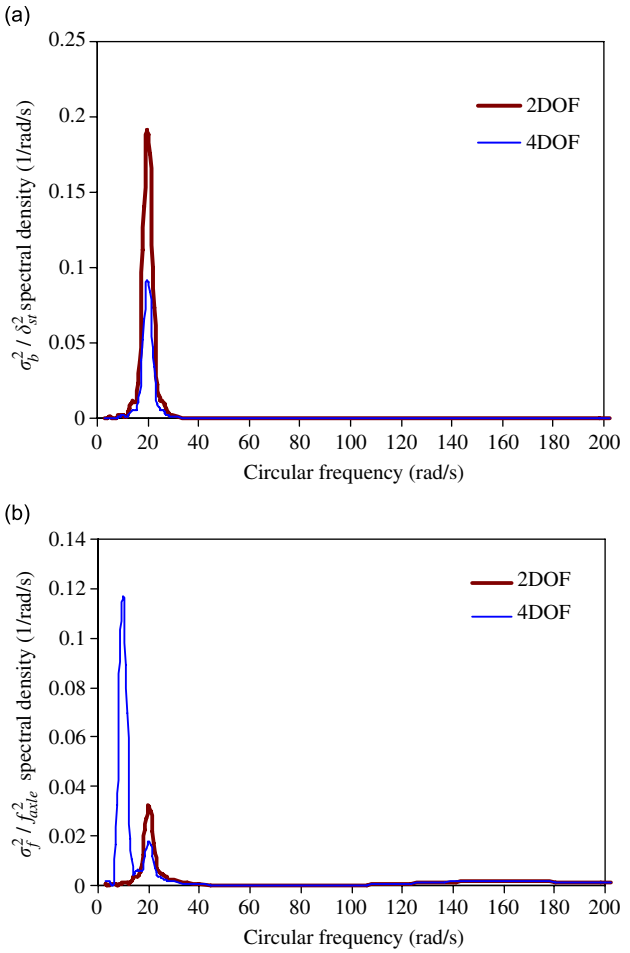

Fig. 9. Spectral densities of the bridge displacement and axle forces: (a) mid-span displacement power spectral density of the bridge and (b) power spectral density of the vehicle axle forces.

vehicle load

$$\mathrm{DAF} = \frac{\delta_{\mathrm{dyn}}}{\delta_{\mathrm{st}}} \tag{26}$$

5.1. *Effect of road surface roughness*

The parameters of the vehicle and bridge models are the same as Example 2 in Section 4. Five different road surface conditions, namely smooth, very good, good, average and poor road surface conditions are used in the calculation to study the effect of the road surface roughness on DAF and DLC. Five different vehicle speeds in the range of 15–35 m/s are considered in the analysis. Figs. 11 and 12, respectively, show the DAF and DLC when the vehicle travels through the bridge of different surface conditions with different speeds. DLC for rear axle has about the same value as the front axle in this example and therefore only the DLC for front axle is plotted in Fig. 12. The results show that both of the DAF and DLC are close to unity for a smooth road surface condition. The maximum DAF and DLC are 1.02 and 1.03 when the vehicle speed is 35 m/s, indicating the dynamic effect is small when the bridge surface is smooth. At the same vehicle speed, the DAF and DLC values increase when the road surface condition changes from smooth to poor. When the vehicle speed is 35 m/s, the DAF is 1.02 for smooth surface condition, 1.21, 1.40, 1.78 and 2.56 for very good, good, average

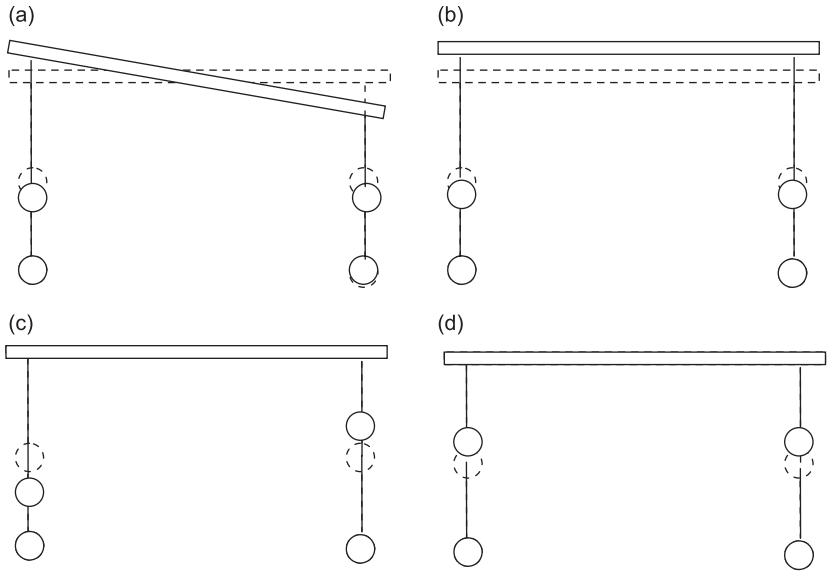

Fig. 10. Frequencies and mode shapes of the 4-DOF vehicle.

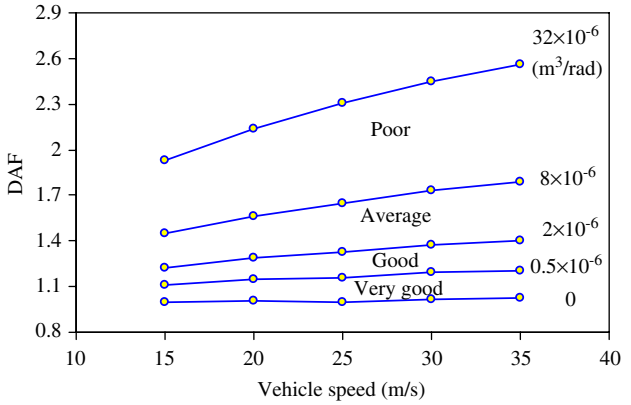

Fig. 11. DAF for different road surface condition.

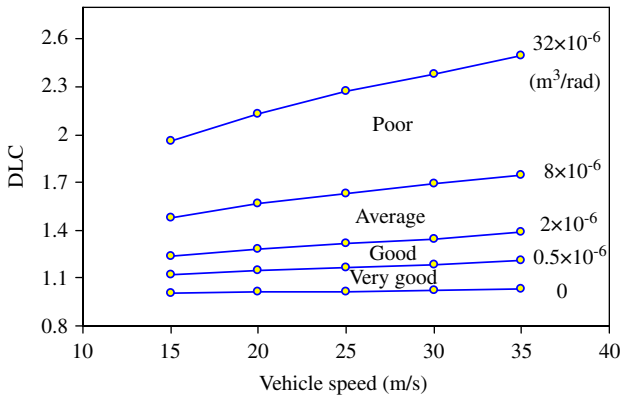

Fig. 12. DLC for different road surface conditions.

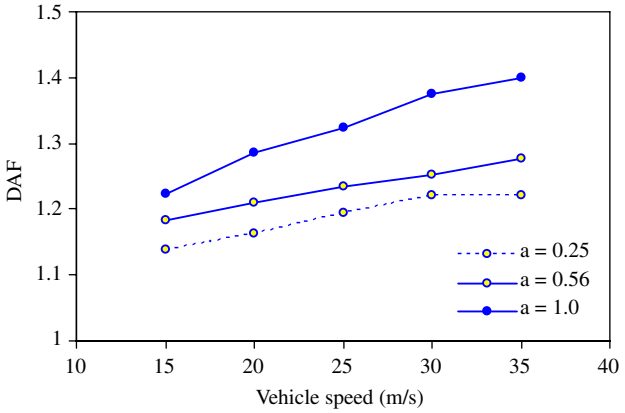

Fig. 13. DAF for different vehicle bridge frequency ratios.

and poor surface condition, respectively. These observations indicate the dynamic effects caused by road surface roughness increase the bridge displacement by 19, 38, 76 and 154 percent of δ_{st}. Similarly, DCL is 1.03 for smooth surface condition, but is 1.21, 1.39, 1.75 and 2.49 for very good, good, average and poor surface condition, when the vehicle speed is 35 m/s, indicating the dynamic effects by road surface roughness cause an increase in the vehicle axle loads by 18, 36, 72 and 146 percent of P_{st}. This is because, as given in Table 1, that the road roughness coefficient increases by four times when the road surface condition decreases to the next class. The change of DAF and DLC are proportional to the squared value of the change of the roughness coefficient. The same conclusion can be drawn from Eqs. (19)–(21). In Eq. (19), the covariance of the bridge displacement is proportional to the road surface roughness coefficient. According to the definition of DAF in Eq. (26), the increment of DAF is proportional to the squared value of $S_d(\Omega)$.

5.2. *Effect of the vehicle to bridge frequency ratio*

The vehicle and bridge model parameters in Example 2 are used to study the effect of the bridge fundamental frequency on DAF and DLC. The change of bridge fundamental frequency is achieved by changing the bridge length. The body bouncing frequency of the vehicle is 3.18 Hz. The fundamental frequency of the bridge is 3.18 Hz for 40 m long bridge, 5.66 Hz for 30 m long bridge and 12.72 Hz for 20 m long bridge. Consequently, the vehicle to bridge frequency ratio, a is 1.0, 0.56 and 0.25. The DAF and DLC for different frequency ratios are plotted in Figs. 13 and 14. It is seen that the maximum value of DAF for each vehicle speed occurs when the frequency ratio is 1.0. The maximum value of DAF is 1.40 when the vehicle passes through a bridge with a good surface condition at 35 m/s. The maximum DAF is 1.22 for frequency ratio 0.25. This observation indicates that resonance between vehicle and bridge causes larger bridge responses as expected. However, the change of the fundamental frequency of the bridge has insignificant influence on vehicle responses, therefore the maximum magnitude of the vehicle axle load as shown in Fig. 14 is almost independent of the bridge vibration frequency.

5.3. *Effect of the length ratio between the vehicle and bridge*

To study the effect of the length ratio between the vehicle and bridge, the vehicle axle spacing is varied from 2 to 6 m while the bridge length remains unchanged as 40 m to avoid changing the bridge fundamental frequency. The vehicle and bridge parameters in Example 2 are used in the analysis. The vehicle axle spacing is taken as 2, 4 and 6 m. Corresponding to different axle spacing, I_v is taken as 144×10^3, 576×10^3 and 1293×10^3 kg m^2 to keep the frequencies of the vehicle unchanged. The vehicle bridge length ratio is 0.05, 0.1 and 0.15. Road surface condition is assumed as good. The DAF and DLC are plotted in Figs. 15 and 16. It is seen that the vehicle axle spacing has insignificant influence on the DLC, while the DAF increases with the

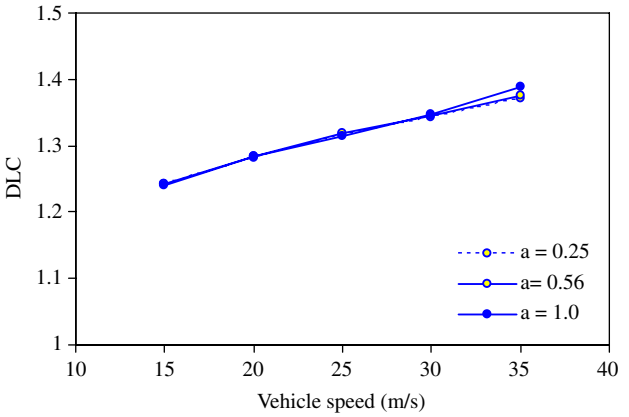

Fig. 14. DLC for different vehicle bridge frequency ratio.

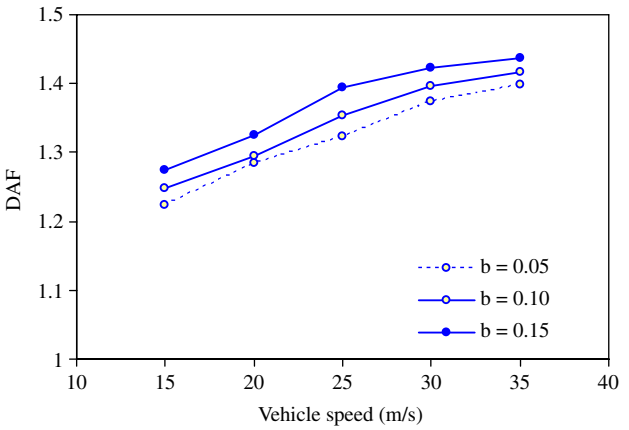

Fig. 15. DAF for different length ratio.

axle spacing because of the normalization although the maximum bridge displacement decreases with the axle spacing. For example, when the vehicle speed is 35 m/s, the DAF is 1.40, 1.42 and 1.44 when the axle spacing is 2, 4 and 6 m. The maximum static mid-span displacement of the bridge from Eq. (24a) is 4.1, 4.0 and 3.8 mm for different axle spacing. The maximum dynamic displacement of the bridge is 5.74, 5.68 and 5.47 mm. It is noted that the influence of different length ratios caused by various axle spacing on the DAF and DLC are less than 3 percent.

5.4. *Effect of the vehicle speed*

As shown in Figs. 11–16, the DAF and DLC increase with the vehicle speed for all the cases considered in the analyses irrespective of the bridge fundamental frequency and vehicle axle spacing, indicating the significant effect of vehicle speed on dynamic vehicle–bridge interaction. This is straightforwardly explained by substituting Eq. (10) into Eq. (19), with the relationship of $\Omega = \omega/v$, the covariance matrix of response becomes

$$E[\mathbf{z}_r(t)\mathbf{z}_r(t)^{\mathrm{T}}] = \int_{-\infty}^{+\infty} vS_d(\Omega_0)\left(\frac{\omega}{\Omega_0}\right)^{-2} G(t,\omega)\,d\omega \tag{27}$$

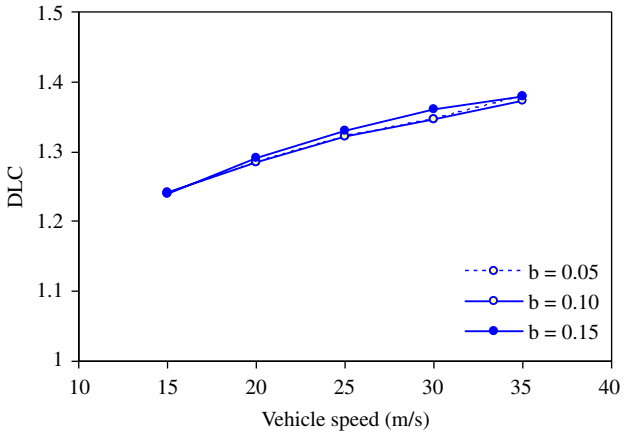

Fig. 16. DLC for different length ratio.

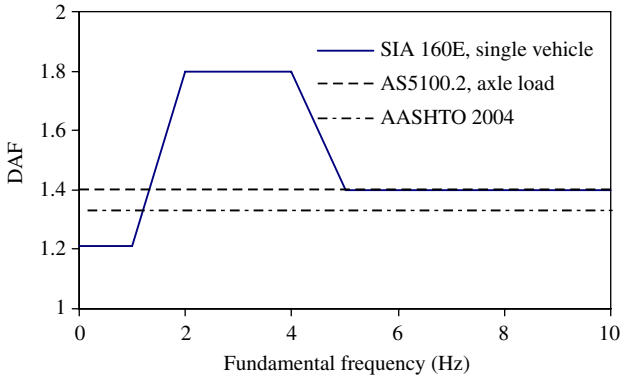

Fig. 17. DAF from different national codes.

where

$$G(t,\omega) = \mathbf{Q}_1(t,\omega)\bar{\mathbf{Q}}_1^{\mathrm{T}}(t,\omega) + \mathrm{i}\omega\mathbf{Q}_1(t,\omega)\bar{\mathbf{Q}}_2^{\mathrm{T}}(t,\omega) - \mathrm{i}\omega\mathbf{Q}_2(t,\omega)\bar{\mathbf{Q}}_1^{\mathrm{T}}(t,\omega) + \omega^2\mathbf{Q}_2(t,\omega)\bar{\mathbf{Q}}_2^{\mathrm{T}}(t,\omega)$$

$$\mathbf{Q}_1(t,\omega) = \int_0^t \mathbf{H}(t,\tau)\mathbf{S}_k(\tau)\mathrm{e}^{-\mathrm{i}\omega\tau}\,\mathrm{d}\tau; \quad \bar{\mathbf{Q}}_1(t,\omega) = \int_0^t \mathbf{H}(t,\tau)\mathbf{S}_k(\tau)\mathrm{e}^{\mathrm{i}\omega\tau}\,d\tau$$

$$\mathbf{Q}_2(t,\omega) = \int_0^t \mathbf{H}(t,\tau)\mathbf{S}_c(\tau)\mathrm{e}^{-\mathrm{i}\omega\tau}\,\mathrm{d}\tau; \quad \bar{\mathbf{Q}}_2(t,\omega) = \int_0^t \mathbf{H}(t,\tau)\mathbf{S}_c(\tau)\mathrm{e}^{\mathrm{i}\omega\tau}\,d\tau$$

Eq. (27) clearly indicates that the DAF and DLC increase with the vehicle speed.

6. Comparison of DAF with code values

Fig. 17 shows different DAF values versus bridge fundamental frequencies provided by AASHTO [1,5] and SIA 160E [25]. The AASHTO load and resistance factor design specifications recommend a DAF of 1.33 for dynamic increment. The Australian Standard [5] provides a uniform value of 1.4 for increment of static wheel and axle load. The DAF value in Switzerland standard [25] is 1.8 in the frequency range of 2–4 Hz and 1.4 when the fundamental frequency of the bridge is greater than 5 Hz.

In Figs. 13 and 15, the maximum DAF is 1.44 when the vehicle and bridge frequency ratio is 1.0 and the vehicle speed is 35 m/s. Based on the relationship between DAF and road surface condition in Fig. 11,

the maximum DAF for average road surface condition is 1.85. According to test by Honda et al. [15], most bridge surfaces are in good to average condition. Therefore, the DAF recommended by AASHTO may underestimate the dynamic increment of the bridge response induced by the road surface roughness, especially when vehicle resonates with bridge. It is well known that the majority of the highway bridges have fundamental frequency in the range of 2–5 Hz, corresponding to the resonant frequencies of commercial vehicles [22]. Therefore, resonance between vehicle and bridge is not unlikely. DAF recommended by AS 5100.2 [5] covers the good road surface condition but may underestimate DAF for bridges with average to poor road surface condition. SIA 160E [25] provides a good estimation of the DAF for most bridges.

7. Conclusions

An evolutionary spectral method has been developed to analyse the dynamic response of the vehicle–bridge system. The deterministic response induced by the vehicle weight and the random response induced by the road surface roughness are calculated separately. The effects of the vehicle speed, bridge fundamental frequency, road surface roughness and axle spacing on the dynamic load are discussed. The results show that the bridge surface roughness is the main factor that causes the dynamic vehicle load on the bridge. The increment of DAF and DLC is proportional to the grade of road surface roughness coefficient. Smooth road surface assumption may lead to substantial underestimation of the DAF and DLC. Bridge fundamental frequency has significant effect on the DAF, and vehicle axle spacing has insignificant effect on both DAF and DLC. The DAF and DLC normally increase with the vehicle speed. It should be noted that the effect of vehicle to bridge mass ratio is not considered in the current study. Vehicle to bridge mass ratio may also affect the vehicle–bridge interaction, which will be a topic of further study.

Acknowledgement

The first author would like to thank the IPRS scholarship to pursue a Ph.D. study in UWA.

Appendix A

$$E[\mathbf{r}(\tau)\mathbf{r}^{\mathrm{T}}(\xi)] = E\begin{bmatrix} r(\hat{x}_1(\tau))r(\hat{x}_1(\xi)) & r(\hat{x}_1(\tau))r(\hat{x}_2(\xi)) \\ r(\hat{x}_2(\tau))r(\hat{x}_1(\xi)) & r(\hat{x}_2(\tau))r(\hat{x}_2(\xi)) \end{bmatrix} \tag{A.1}$$

$\hat{x}_1(t)$ is the distance from the end of the bridge to the front axle and $\hat{x}_2(t)$ is the distance from the end of the bridge to the rear axle at t. Assume the $r(\hat{x}_1(t))$ is statistically independent of $r(\hat{x}_2(t))$, it has

$$E[r(\hat{x}_1(\tau))r(\hat{x}_2(\xi))] = E[r(\hat{x}_2(\tau))r(\hat{x}_1(\xi))] = 0 \tag{A.2}$$

$$E[r(\hat{x}_1(\tau))r(\hat{x}_1(\xi))] = \int_{-\infty}^{\infty} S(\omega)\,\exp[\mathrm{i}\omega(\hat{x}_1(\xi) - \hat{x}_1(\tau))]\,d\omega \tag{A.3}$$

Since $x_2(t) = x_1(t) - S$

$$E[r(\hat{x}_2(\tau))r(\hat{x}_2(\xi))] = \int_{-\infty}^{\infty} S(\omega)\,\exp[\mathrm{i}\omega(\hat{x}_2(\xi) - \hat{x}_2(\tau))]\,d\omega = E[r(\hat{x}_1(\tau))r(\hat{x}_1(\xi))] \tag{A.4}$$

$$E[\mathbf{r}(\tau)\mathbf{r}^{\mathrm{T}}(\xi)] = \mathbf{\Lambda}\int_{-\infty}^{\infty} S(\omega)\,\exp[\mathrm{i}\omega(\hat{x}_1(\xi) - \hat{x}_1(\tau))]\,d\omega \tag{A.5}$$

where

$$\Lambda = \begin{bmatrix} 1 & 0 \\ 0 & 1 \end{bmatrix}$$

$$E[\mathbf{r}(\tau)\mathbf{r}'^{\mathrm{T}}(\xi)] = E\begin{bmatrix} r(\hat{x}_1(\tau))r'(\hat{x}_1(\xi)) & r(\hat{x}_1(\tau))r'(\hat{x}_2(\xi)) \\ r(\hat{x}_2(\tau))r'(\hat{x}_1(\xi)) & r(\hat{x}_2(\tau))r'(\hat{x}_2(\xi)) \end{bmatrix} \tag{A.6}$$

$$E[r(\hat{x}_1(\tau))r'(\hat{x}_1(\xi))] = \frac{\partial E[r(\hat{x}_1(\tau))r(\hat{x}_1(\xi))]}{\partial \hat{x}_1(\xi)} = \int_{-\infty}^{+\infty} \mathrm{i}\omega S(\omega)\, \exp[\mathrm{i}\omega(\hat{x}_1(\xi) - \hat{x}_1(\tau))]\, d\omega \tag{A.7}$$

$$E[r(\hat{x}_1(\tau))r'(\hat{x}_2(\xi))] = \frac{\partial E[r(\hat{x}_1(\tau))r(\hat{x}_2(\xi))]}{\partial \hat{x}_2(\xi)} = 0 \tag{A.8}$$

$$E[r(\hat{x}_2(\tau))r'(\hat{x}_1(\xi))] = \frac{\partial E[r(\hat{x}_2(\tau))r(\hat{x}_1(\xi))]}{\partial \hat{x}_1(\xi)} = 0 \tag{A.9}$$

$$E[r(\hat{x}_2(\tau))r'(\hat{x}_2(\xi))] = E[r(\eta_1)r'(\eta_2)] \tag{A.10}$$

$$E[\mathbf{r}(\tau)\mathbf{r}'^{\mathrm{T}}(\xi)] = \mathbf{\Lambda} \int_{-\infty}^{+\infty} \mathrm{i}\omega S(\omega) \exp[\mathrm{i}\omega(\hat{x}_1(\xi) - \hat{x}_1(\tau)]d\omega \tag{A.11}$$

$$E[\mathbf{r}'(\tau)\mathbf{r}^{\mathrm{T}}(\xi)] = -\mathbf{\Lambda} \int_{-\infty}^{+\infty} \mathrm{i}\omega S(\omega)\, \exp[\mathrm{j}\omega(\hat{x}_2(\xi) - \hat{x}_2(\tau))]\, d\omega \tag{A.12}$$

$$E[\mathbf{r}'(\tau)\mathbf{r}'^{\mathrm{T}}(\xi)] = \mathbf{\Lambda} \int_{-\infty}^{+\infty} \omega^2 S(\omega) \exp[\mathrm{j}\omega(\hat{x}_2(\xi) - \hat{x}_2(\tau))]d\omega \tag{A.13}$$

References

[1] AASHTO, *LRFD Bridge Design Specification*, third ed., American Association of State Highway and Transportation Officials, Washington, DC, USA, 2004.

[2] J.E. Akin, M. Mofid, Numerical solution for response of beams with moving mass, *Journal of Structural Engineering ASCE* 115 (1) (1989) 120–131.

[3] D.B. Ashebo, T.H.T. Chan, L. Yu, Evaluation of dynamic loads on a skew box girder continuous bridge part II: parametric study and dynamic load factor, *Engineering Structures* 29 (2007) 1064–1073.

[4] F.T.K. Au, Y.S. Cheng, Y.K. Cheung, Effects of random road surface roughness and long-term deflection of prestressed concrete girder and cable-stayed bridges on impact due to moving vehicles, *Computers and Structures* 79 (2001) 853–872.

[5] Australian Standard AS5100.2, *Bridge Design Part 2: Design Loads*, Standards Australia International Ltd., Sydney, 2004.

[6] C. Bilello, L.A. Bergman, D. Kuchma, Experimental investigation of a small-scale bridge model under a moving mass, *Journal of Structural Engineering ASCE* 130 (5) (2004) 799–804.

[7] S.P. Brady, E.J. O'Brien, A. Znidaric, Effect of vehicle velocity on the dynamic amplification of a vehicle crossing a simple supported bridge, *Journal of Bridge Engineering ASCE* 11 (2) (2006) 241–249.

[8] P.K. Chatterjee, T.K. Datta, C.S. Surana, Vibration of suspension bridges under vehicular movement, *Journal of Structural Engineering ASCE* 120 (3) (1994) 681–703.

[9] T.H.T. Chan, L. Yu, T.H. Yung, J.H.F. Chan, A new bridge–vehicle system part I: formulation and validation, *Structural Engineering and Mechanics* 15 (1) (2003) 1–19.

[10] T.H.T. Chan, L. Yu, T.H. Yung, J.H.F. Chan, A new bridge–vehicle system part II: parametric study, *Structural Engineering and Mechanics* 15 (1) (2003) 21–38.

[11] L. Fryba, Non-stationary response of a beam to a moving random force, *Journal of Sound and Vibration* 46 (3) (1976) 323–338.

[12] L. Fryba, *Vibration of Solids and Structures under Moving Loads*, Thomas Telford Ltd., London, 1999.

[13] M.F. Green, D. Cebon, Dynamic response of highway bridges to heavy vehicle loads: theory and experimental validation, *Journal of Sound and Vibration* 170 (1) (1994) 51–78.

[14] K. Henchi, M. Fafard, M. Talbot, G. Dhatt, An efficient algorithm for dynamic analysis of bridges under moving vehicles using a coupled modal and physical components approach, *Journal of Sound and Vibration* 212 (4) (1998) 663–683.

[15] H. Honda, Y. Kajikawa, T. Kobori, Spectra of road surface roughness on bridges, *Journal of the Structural Division, ASCE* 108 (ST9) (1982) 1956–1966.

[16] International Organization for Standardization ISO 8608 (1995). Mechanical Vibration—Road Surface Profiles—Reporting of Measured Data, Switzerland.

[17] E.S. Hwang, A.S. Nowak, Simulation of dynamic load for bridges, *Journal of Structural Engineering* 117 (5) (1991) 1413–1434.

[18] C.W. Kim, M. Kawatani, K.B. Kim, Three-dimensional dynamic analysis for bridge–vehicle interaction with roadway roughness, *Computers and Structures* 83 (2005) 1627–1645.
[19] S.S. Law, X.Q. Zhu, Bridge dynamic responses due to road surface roughness and breaking of vehicle, *Journal of Sound and Vibration* 282 (2005) 805–830.
[20] J.Q. Li, X.L. Leng, T. Fang, Evolutionary random response problem of a coupled vehicle–bridge system, *Archive of Applied Mechanics* 72 (2002) 536–544.
[21] J.H. Lin, C.C. Weng, Evaluation of dynamic vehicle load on bridge deck, *Journal of the Chinese Institute of Engineers* 27 (5) (2004) 695–705.
[22] P. Paultre, O. Chaallal, J. Proulx, Bridge dynamics and dynamic amplification factors—a review of analytical and experimental findings, *Canadian Journal of Civil Engineering* 19 (1992) 260–278.
[23] A.V. Pesterev, L.A. Bergman, C.A. Tan, A novel approach to the calculation of pothole-induced contact forces in MDOF vehicle models, *Journal of Sound and Vibration* 275 (2004) 127–149.
[24] M. Samaan, J.B. Kennedy, K. Sennah, Impact factor for curved continuous composite multiple-box girder bridge, *Journal of Bridge Engineering ASCE* 12 (1) (2007) 80–88.
[25] SIA 160E, *Einwirkungen auf Tragwerke, Entwurf, Schweiz, Ingenieur und Architekten-verein*, Zurich, Switzerland, 1988.
[26] N. Sridharan, A.K. Mallik, Numerical analysis of vibration of beams subjected to moving loads, *Journal of Sound and Vibration* 65 (1) (1979) 147–150.
[27] T.L. Wang, D.Z. Huang, Cable-stayed bridge vibration due to road surface roughness, *Journal of Structural Engineering ASCE* 118 (5) (1992) 1354–1374.
[28] H.S. Zibdeh, Stochastic vibration of an elastic beam due to random moving loads and deterministic axial forces, *Engineering Structures* 17 (7) (1995) 530–535.